GEOPHYSICS, VOL. 70, NO. 5 (SEPTEMBER-OCTOBER 2005); P. S79–S89, 18 FIGS.
10.1190/1.2052471

Least-squares joint imaging of multiples and primaries

Morgan P. Brown[1] and Antoine Guitton[2]

ABSTRACT

Multiple reflections contain subsurface reflectivity information which often complements that found in primary reflections. Previous attempts to combine the additional information by summing prestack images of the primaries and multiples have generally failed because of crosstalk leakage between the images. We present a general linear least-squares joint imaging of multiples and primaries (LSJIMP) inversion method to simultaneously suppress crosstalk noise and combine pegleg multiples and primaries in a prestack sense. In general, LSJIMP is compatible with a wide variety of prestack imaging methods and can be extended to jointly image primaries and other embedded wave modes such as shear-wave conversions.

We present a particular LSJIMP implementation that utilizes an efficient linear operator to model and image pegleg multiples in a true relative-amplitude sense. Applied to a given type of pegleg multiple in the data, our imaging operator produces an image directly comparable to primaries after NMO. Our operator's kinematic component is an extension of the NMO equation that independently images split peglegs in a moderately heterogeneous earth. Its amplitude component corrects multiples for their differences in angle-dependent reflection strength and illumination, relative to a primary. We test our LSJIMP implementation on 2D and 3D prestack field data examples and show that the method cleanly separates primaries and multiples and also uses joint information in the events to interpolate the signal in acquisition gaps.

INTRODUCTION

Seismic data acquired in marine environments almost always contain observable multiple reflections from the air-water interface. Multiples may significantly impede the construction and interpretation of an image of the primaries, especially in regions with strong reflectors (e.g., hard water bottom or salt bodies). Multiple suppression techniques have, by necessity, advanced contemporaneously with reflection imaging for many years.

Despite its usual classification as noise, however, energy from multiples often penetrates deeply enough into the earth to illuminate the prospect zone. In this sense, the multiples can be viewed as a perfectly viable signal, rather than noise. Moreover, since they illuminate different angular ranges and reflection points (see Figure 1), a primary and its multiples are more than redundant. In theory and in practice, multiples provide subsurface information not found in the primaries.

To use the new information provided by multiples, one must first map the multiples and primaries to a domain where they are directly comparable and then combine them in some fashion. Imaging algorithms such as migration reduce the signal — either primaries or multiples — to a compact form by removing the effects of wave propagation through the overburden. Additionally, if the prestack primary and multiple images are arranged in angle-domain common-image gathers (CIGs) [e.g., Sava and Fomel (2003)], the events can be analyzed jointly for angle-dependent phenomena. Thus, the angle domain after prestack imaging represents a natural domain in which to combine multiples and primaries.

An important class of multiple suppression techniques predicts multiples by adding a multiple bounce to the recorded data with wavefield extrapolation (Morley, 1982; Berryhill and Kim, 1986; Wiggins, 1988; Lu et al., 1999) or with autoconvolution (Riley and Claerbout, 1976; Tsai, 1985; Verschuur et al., 1992). Conversely, reversing the extrapolation direction removes a multiple bounce from the data and transforms pegleg multiples into pseudo-primary events (Berkhout and Verschuur, 2003; Shan, 2003). While conventional migration can image the pseudo-primaries (Shan, 2003), most published multiple-imaging techniques perform the reverse modeling process implicitly and image the multiples directly with Kirchhoff migration (Reiter et al., 1991; He and Schuster, 2003)

Manuscript received by the Editor May 21, 2004; revised manuscript received March 14, 2005; published online September 8, 2005.
[1]Formerly Stanford University, Department of Geophysics, Stanford, California 94305-2215; presently Amerada Hess Corporation, 500 Dallas St., Houston, Texas 77002. E-mail: mpbrown@hess.com.
[2]Stanford University, Department of Geophysics, 397 Panama Mall, Stanford, California 94305-2215. E-mail: antoine@sep.stanford.edu.
© 2005 Society of Exploration Geophysicists. All rights reserved.

or wave-equation (Berkhout and Verschuur, 1994; Yu and Schuster, 2001; Guitton, 2002).

These techniques correctly image multiples to the position of an equivalent primary, but they fail to seriously tackle the equally important problem of combining the multiple and primary images. Primaries and each mode of multiples constitute semi-independent measurements of the earth's reflectivity; unfortunately, they overlap one another in a single data record. Summing the primary and multiple images (Reiter et al., 1991; Berkhout and Vershuur, 1994; Shan, 2003) could potentially improve signal-to-noise ratio (S/N) and fill illumination gaps, but this strategy encounters a significant problem. Just as multiples constitute noise on the primary image, primaries and higher-order multiples constitute noise on the first-order multiple image (Figure 2). We refer to these contamination events as crosstalk (Claerbout, 1992). Corresponding crosstalk events on the primary and multiple images have similar kinematics, so summing the images does little to increase S/N or to improve signal fidelity unless the individual modes are separated before imaging and combination. Unfortunately, cleanly separating a variety of different multiple modes from prestack data is both expensive and difficult. Moreover, if mode separation is performed as a preprocessing step, amplitude bias in the separated modes will likely inhibit the later integration of primaries and multiples.

In this paper we introduce the least-squares joint imaging of multiples and primaries (LSJIMP) method, which aims to solve the separation and integration problems simultaneously as a global least-squares inversion. The model space of the inverse problem (Figure 3) consists of images corresponding to primaries and to each important multiple mode. Correct partitioning of the energy from each mode into one and only one image implies that (1) multiples and primaries have been separated and that (2) the modeled data fit the recorded data. However, because the inverse problem is underdetermined, minimizing the modeling error alone does not ensure a correct partitioning of energy, since forward-modeled crosstalk is indistinguishable from forward-modeled signal (see Figure 4). To overcome this problem, we devise three model-regularization operators that discriminate

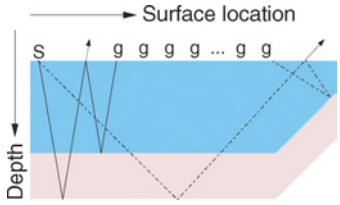

Figure 1. Small-angle and far-angle reflectivity information contained in multiples but not in primaries.

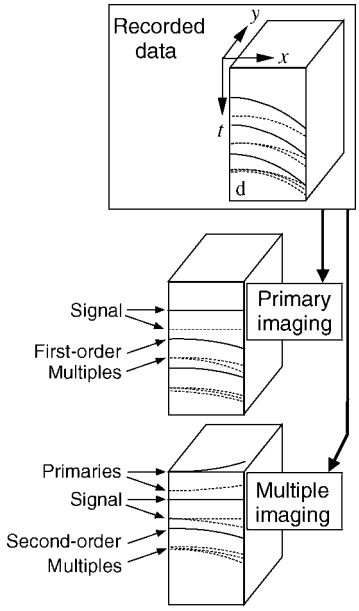

Figure 2. Illustration of crosstalk on images of primaries and multiples. On the primary image, signal events are primaries; everything else is crosstalk. On the multiple image, signal events are first-order, receiver-side multiples; everything else is crosstalk. Corresponding crosstalk events are quite consistent between images, so summing them will not markedly increase S/N or signal fidelity.

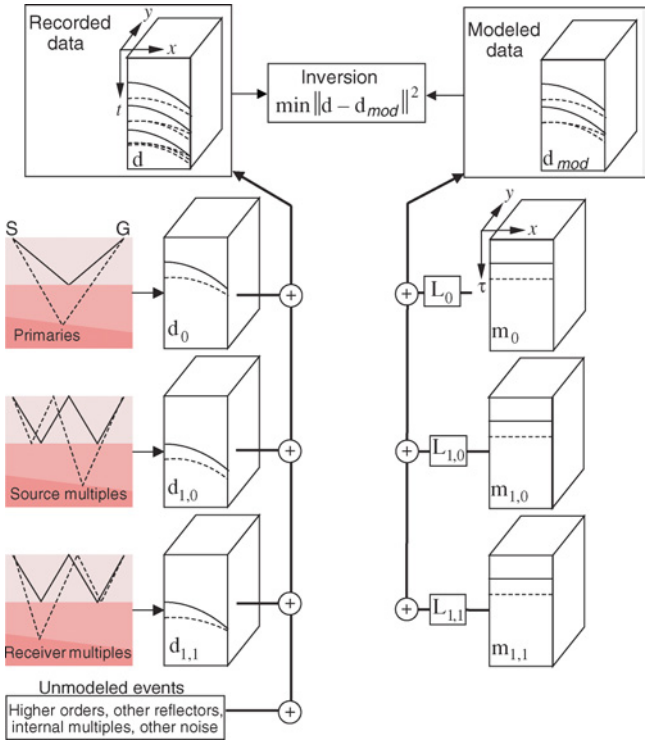

Figure 3. LSJIMP schematic. Assume that the recorded data consist of primaries and pegleg multiples. Here, we model only first-order source-side and receiver-side peglegs with the multiple bounce on the shallow reflector. By definition, the images $\mathbf{m}_{i,k}$ contain only energy from a specific multiple mode $\mathbf{d}_{i,k}$ and are consistent with the other $\mathbf{m}_{i,k}$ with respect to both kinematics and amplitudes. Indices i and k correspond to multiple order and type (source side or receiver side). $\mathbf{L}_{i,k}$ maps events in $\mathbf{m}_{i,k}$ to events that should fit recorded events $\mathbf{d}_{i,k}$. The LSJIMP inversion adjusts $\mathbf{m}_{i,k}$ to fit the recorded data $\mathbf{d}$ in a least-squares sense. Model-regularization operators suppress the crosstalk in each $\mathbf{m}_{i,k}$ and exploit the intrinsic redundancy between and within the images to increase signal fidelity and fill illumination gaps.

crosstalk from signal and thereby properly partition each mode's energy into the correct image.

The model-regularization operators serve a higher purpose than crosstalk suppression alone, however, and represent the novelty of the LSJIMP method. Differential operators applied across the reflection angle and between images spread signals from other angles or images to fill illumination gaps and increase signal fidelity. By exploiting an additional, previously ignored dimension of data redundancy — that between primaries and multiples — we can, with a degree of rigor, claim to have solved a joint imaging problem and actually to have used the multiples constructively. LSJIMP's use of multiples to constrain the least-squares imaging problem is a novel generalization of existing regularized, least-squares prestack imaging schemes that exploit signal redundancy across the reflection angle to fill illumination gaps (Kuehl and Sacchi, 2001; Prucha-Clapp and Biondi, 2002; Wang et al., 2003).

LSJIMP INVERSE PROBLEM

Generalizing the LSJIMP forward model from Figure 3, we conceptualize the recorded data as the superposition of primary reflections and p orders of pegleg multiples from n_{surf} multiple-generating surfaces. In Figure 3, $p=1$ and $n_{surf}=1$. Whereas a first-order pegleg splits into source-side and receiver-side legs, an ith-order pegleg splits into $i+1$ legs. Denoting the primaries as $\mathbf{d}_0$ and the kth leg of the ith-order pegleg from the mth multiple generator as $\mathbf{d}_{i,k,m}$, the modeled data take the following form:

$$\mathbf{d}_{mod} = \mathbf{d}_0 + \sum_{i=1}^{p}\sum_{k=0}^{i}\sum_{m=1}^{n_{surf}} \mathbf{d}_{i,k,m}. \tag{1}$$

We can cast $\mathbf{d}_{i,k,m}$ as linear functions of prestack images. Let us denote the modeling operator for primaries as $\mathbf{L}_0$ and the image of the primaries as $\mathbf{m}_0$. Similarly, for the pegleg $\mathbf{d}_{i,k,m}$ we denote the modeling operator and image as $\mathbf{L}_{i,k,m}$ and $\mathbf{m}_{i,k,m}$, respectively. We can now rewrite equation 1 as

$$\mathbf{d}_{mod} = \mathbf{L}_0\mathbf{m}_0 + \sum_{i=1}^{p}\sum_{k=0}^{i}\sum_{m=1}^{n_{surf}} \mathbf{L}_{i,k,m}\mathbf{m}_{i,k,m} \tag{2}$$

$$= \mathbf{L}\mathbf{m}. \tag{3}$$

Note that signal events in $\mathbf{m}_0$ and $\mathbf{m}_{i,k,m}$ are assumed consistent with respect both to kinematics and to angle-dependent amplitudes. This assumption implies that signal events are comparable between images and thus implies that $\mathbf{L}_{i,k,m}$ must be true-amplitude modeling operators relative to $\mathbf{L}_0$.

The LSJIMP method optimizes (e.g., using the conjugate gradient method) the primary and multiple images by minimizing the ℓ_2-norm of the data residual, defined as the difference between the recorded data $\mathbf{d}$ and the modeled data:

$$\min_{\mathbf{m}} \|\mathbf{W_d}[\mathbf{d} - \mathbf{L}\mathbf{m}]\|^2, \tag{4}$$

where the residual weighting operator $\mathbf{W_d}$ forces the residual to be independent and identically distributed (*iid*) or, more intuitively, uncorrelated and evenly scaled. Even simpler choices are possible; in our LSJIMP implementation, we choose $\mathbf{W_d}$ as a diagonal weighting operator (0.0 at missing trace locations; 1.0 elsewhere).

Other authors have solved a similar least-squares problem. Nemeth et al. (1999) jointly images and separates compressional waves and various (nonmultiple) embedded coherent noise modes. Guitton et al. (2001) use a prior multiple model and nonstationary prediction-error filters to model primaries and surface-related multiples.

Minimization 4 is generally underdetermined, implying an infinite number of optimal solutions. The nonuniqueness problem is closely related to crosstalk leakage, as illustrated by Figure 4. Recall that all energy from pegleg $\mathbf{d}_{i,k,m}$ must be partitioned to $\mathbf{m}_{i,k,m}$ if we hope to combine the primary and multiple images meaningfully. To better constrain the LSJIMP inversion, we regularize the problem.

LSJIMP regularization

Quite simply, an underdetermined minimization problem has more unknowns than equations; model regularization consists of adding unique equations to the system. More rigorously, model regularization is closely related to the prior model's covariance, or how we believe model parameters depend on one another (Tarantola, 1987). Figure 3 motivates the desired model covariance for the LSJIMP problem. After optimization, the primary and multiple images should contain energy from only one particular primary or multiple mode. In other words, the images should be crosstalk free.

We can rewrite minimization 4 after adding a generic linear model-regularization operator $\mathbf{R}$:

$$\min_{\mathbf{m}} \|\mathbf{W_d}[\mathbf{d} - \mathbf{L}\mathbf{m}]\|^2 + \epsilon\|\mathbf{R}\mathbf{m}\|^2. \tag{5}$$

We call the second term of equation 5 the model residual. Scalar ϵ balances the relative importance of the data and model residuals in the minimization. If we design $\mathbf{R}$ to (counterintuitively) boost unwanted components of $\mathbf{m}$, then to minimize equation 5, a solver will tend to suppress those components.

To the basic LSJIMP inverse problem we add three model-regularization operators, which boost crosstalk energy relative to signal energy. These operators also exploit the signal's

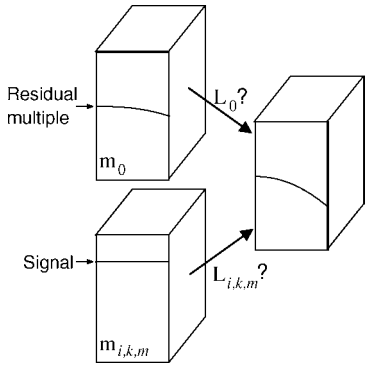

Figure 4. Nonuniqueness of the LSJIMP problem without regularization. Residual multiple energy on $\mathbf{m}_0$ (crosstalk) mapped to data space by $\mathbf{L}_0$ is indistinguishable from a correctly imaged multiple on $\mathbf{m}_{i,k,m}$ (signal) mapped to data space by $\mathbf{L}_{i,k,m}$.

redundancy within and between images to increase signal fidelity and to fill illumination gaps and missing traces.

Differencing across angle

After prestack imaging with the correct velocity, signal events are flat with angle/offset, while crosstalk events generally have residual moveout. Provided that the signal's amplitude-versus-angle (AVA) response varies slowly, a differencing operator applied across angle tends to boost crosstalk amplitude but not signal amplitude. We denote this operator $\mathbf{D_h}$. Other authors use similar methodologies to penalize illumination gaps in least-squares prestack migration (Kuehl and Sacchi, 2001; Prucha-Clapp and Biondi, 2002; Wang et al., 2003). If a signal event is not flat, $\mathbf{D_h}$ will damage it in the LSJIMP inversion. Conversely, $\mathbf{D_h}$ cannot distinguish crosstalk from signals at near angles/offsets, where both events are usually flat.

Differencing between images

After prestack imaging, signal events on the primary and multiple images are by definition consistent with respect to kinematics and amplitudes. Conversely, corresponding crosstalk events on two images (e.g., first-order multiples on $\mathbf{m}_0$ and second-order multiples on $\mathbf{m}_{i,k,m}$) generally have different residual moveout. The moveout differences are usually small at near angles/offsets but increase at far offsets and in the presence of subsurface complexity (Brown, 2004). Where the moveout differences are larger than a quarter of a wavelength, a differencing operator applied between images tends to boost crosstalk amplitude but not signal amplitude. We denote this operator $\mathbf{D_m}$.

A central motivation for LSJIMP is the desire to combine information from the multiple and primary images by averaging. As a regularization operator, $\mathbf{D_m}$ accomplishes the averaging by penalizing differences between images. Additionally, because the averaging occurs within the framework of a least-squares minimization, we can combine the multiples and primaries as well as quantitatively fit the data.

In using $\mathbf{D_m}$, we assume that signal events on all images are perfectly consistent. Imperfections in the modeling operator $\mathbf{L}_{i,k,m}$ lead to differences in the signal events, which violate this assumption and cause $\mathbf{D_m}$ to damage signal events.

Both the primary and multiple images have acquisition gaps. When implementing LSJIMP, $\mathbf{D_m}$ should be supplemented with an appropriate diagonal weighting operator that reflects the local information content of an image. For example, at far angles/offsets, multiples usually carry little information, so the weighting operator would nullify the output of $\mathbf{D_m}$ there.

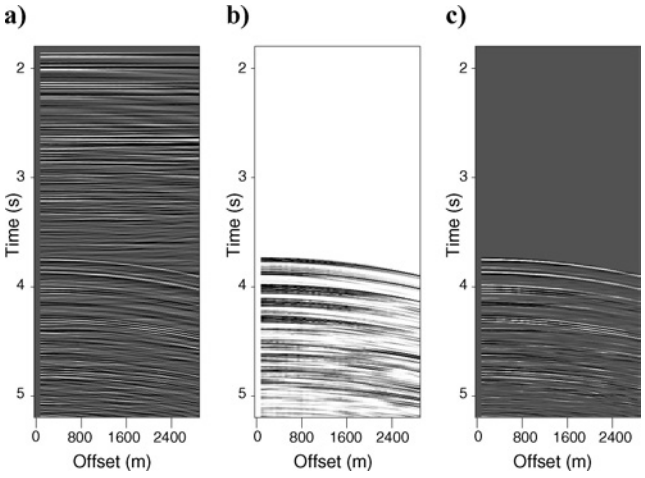

Figure 5. Application of crosstalk weights to a real CMP gather after prestack imaging. (a) Primary image $\mathbf{L}_0^T\mathbf{d}$. (b) Crosstalk weight $|\mathbf{c}_0|$. (c) Weighted image $|\mathbf{c}_0|\mathbf{L}_0^T\mathbf{d}$.

Crosstalk penalty weights

Given a prior signal estimate $\mathbf{m}^{[p]}_{i,k,m}$, we can directly model the expected crosstalk events on all $\mathbf{m}_{i,k,m}$. Applying $\mathbf{L}_{i,k,m}$ to $\mathbf{m}^{[p]}_{i,k,m}$ yields an estimate of the $\{i, k, m\}$ pegleg. Imaging this estimated pegleg as if it were a different multiple — say, by applying $\mathbf{L}^T_{i',k',m'}$ — in turn yields an estimate of the crosstalk from the $\{i, k, m\}$ multiple on $\mathbf{m}_{i',k',m'}$. We then sum over all $\{i, k, m\}$ to obtain the total estimated crosstalk on $\mathbf{m}_{i',k',m'}$, which we denote as

$$\mathbf{m}^{[c]}_{i',k',m'} = \sum_{i=i_0}^{p}\sum_{k=0}^{i}\sum_{m=1}^{n_{surf}} \mathbf{L}^T_{i',k',m'}\mathbf{L}_{i,k,m}\mathbf{m}^{[p]}_{i,k,m},$$

$$\text{where } k \neq k',\ m \neq m' \text{ and } i_0 = \begin{cases} 1 & \text{if } i' = 0 \\ i & \text{otherwise} \end{cases}. \quad (6)$$

We convert each $\mathbf{m}^{[c]}_{i',k',m'}$ into a diagonal weighting function by computing the absolute value and denote this as operator $\mathbf{D_c}$. While $\mathbf{D_h}$ and $\mathbf{D_m}$ tend to suppress crosstalk at far angles only, $\mathbf{D_c}$ suppresses crosstalk at all angles.

Strictly speaking, we lack a prior signal estimate without performing a nonlinear iteration (Brown, 2004). However, between the seabed reflection and its first multiple, the recorded data effectively contain only primaries, so we can limit the crosstalk prediction to events arising from multiple generators above the first seabed multiple. This assumption particularly applies to deep-water marine data.

Although the crosstalk weights overlap (and damage) signal events on any image, the previous regularization operators ($\mathbf{D_h}$ and $\mathbf{D_m}$) spread redundant signal information from other images and other angles/offsets to compensate for any losses. Figure 5 illustrates the application of the crosstalk weights to the primary image $\mathbf{m}_0$. The weights clearly boost the energy of the crosstalk events (multiples).

We can now rewrite the general regularized LSJIMP minimization 5 using the three regularization operators:

$$\min_{\mathbf{m}} Q(\mathbf{m}) = \|\mathbf{W_d}[\mathbf{Lm} - \mathbf{d}]\|^2 + \epsilon_1^2\|\mathbf{D_h m}\|^2 + \epsilon_2^2\|\mathbf{D_m m}\|^2 + \epsilon_3^2\|\mathbf{D_c m}\|^2. \quad (7)$$

Effectively, $\mathbf{R}$ in equation 5 is replaced by the column operator $[\mathbf{D_h}\ \mathbf{D_m}\ \mathbf{D_c}]^{\mathbf{T}}$, while ϵ_1, ϵ_2, and ϵ_3 replace ϵ. A method for quantitatively choosing ϵ_1, ϵ_2, and ϵ_3 remains a subject of research. Qualitatively, high values lead to good crosstalk suppression and some damage to signal events, while low values

lead to good signal preservation and poor crosstalk suppression.

PARTICULAR LSJIMP IMPLEMENTATION

In this section, we present a particular LSJIMP implementation that utilizes an efficient linear operator to model and image pegleg multiples in a true-relative-amplitude sense. Applied to primary reflections after NMO, the forward operator models a particular pegleg. Applied to that particular pegleg in the data, the adjoint operator produces events that are directly comparable to primaries after NMO. The operator's kinematic component is an extension of the NMO equation, which images split peglegs. Its amplitude component corrects multiples for their differences in angle-dependent reflection strength, relative to a primary.

Kinematic pegleg imaging in a 1D earth

In a laterally homogeneous earth, the NMO equation describes a primary's traveltime as a function of source-receiver offset:

$$t = \sqrt{\tau + \frac{\|\mathbf{x}\|^2}{V_{\text{rms}}^2(\tau)}}. \tag{8}$$

Applied as an offset-dependent time shift, equation 8 flattens a primary (on a CMP gather) with offset vector $\mathbf{x}$ and rms velocity $V_{\text{rms}}(\tau)$ to its zero-offset traveltime τ.

Figure 6 motivates an analogous NMO equation for pegleg multiples. Kinematically, a first-order pegleg can be conceptualized as a pseudo-primary with the same offset but with an additional zero-offset traveltime τ^* to the multiple generator. We can generalize this intuition to write an NMO equation for an nth-order pegleg:

$$t = \sqrt{(\tau + n\tau^*)^2 + \frac{\|\mathbf{x}\|^2}{V_{eff}^2}}, \tag{9}$$

where

$$V_{eff}^2 = \frac{n\tau^* V_{\text{rms}}^2(\tau^*) + \tau V_{\text{rms}}^2(\tau)}{\tau + n\tau^*}. \tag{10}$$

The pseudo-primary's effective rms velocity, V_{eff}, can be derived easily (Wang, 2003) from the definition of rms velocity. The relative shift of the primary and pegleg reflection points ($\Delta\, y$ in Figure 6) decreases asymptotically to zero for $\tau \to \infty$ from a maximum value at the seabed.

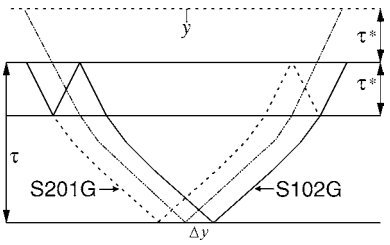

Figure 6. Peglegs S201G and S102G [Levin and Shah's (1977) notation] are kinematically equivalent to a pseudo-primary with extra zero-offset traveltime τ^*.

Amplitude corrections for peglegs

Primaries and multiples recorded at fixed offsets follow different raypaths from source to receiver. Thus, they exhibit different amplitude-versus-offset (AVO) behavior and suffer different attenuation and geometric-spreading losses. We present two operators that normalize (relative to a primary) a pegleg for these effects and a reflection operator that accounts for a multiple's extra bounces.

First, Figure 7 illustrates that in a $v(z)$ medium there exists a vector $\mathbf{x}_p$ such that a pegleg with offset $\mathbf{x}$ and a primary with offset $\mathbf{x}_p$ are invariant with respect to AVO and, ignoring attenuation above the multiple generator (this is often water), also to attenuation. Noting that the multiple and primary in Figure 7 have the same emergence angle and thus the same time dip at $\mathbf{x}$ and $\mathbf{x}_p$, Brown (2004) obtains

$$\mathbf{x}_p = \frac{\mathbf{x}\tau V_{\text{rms}}^2}{\sqrt{(\tau + n\tau^*)^2 V_{eff}^4 + \|\mathbf{x}\|^2 \left(V_{eff}^2 - V_{\text{rms}}^2\right)}} \tag{11}$$

for an nth-order pegleg. Snell resampling is our name for the resampling of the offset axis defined by equation 11. Figure 8 illustrates the process on a synthetic CMP gather. The black lines depict the compression of the offset axis and show how energy from the multiples fills the data coverage gaps.

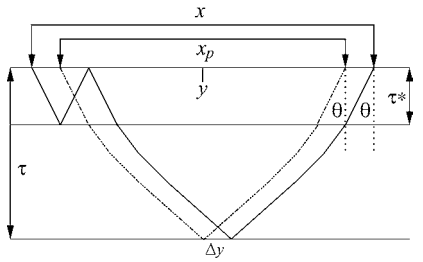

Figure 7. A primary and a pegleg multiple with the same emergence angle θ and midpoint y.

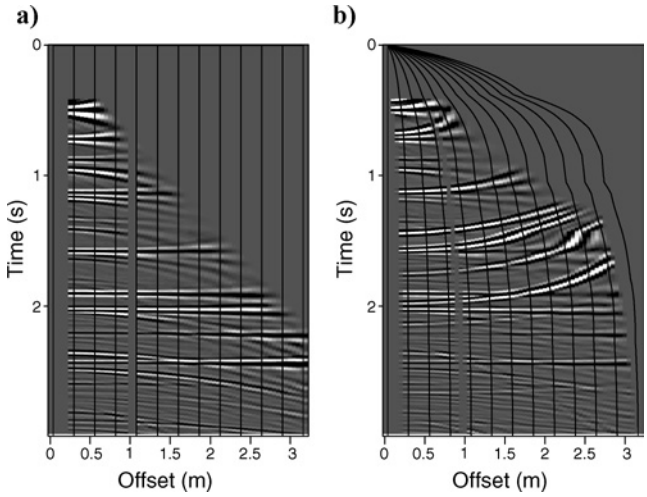

Figure 8. (a) Synthetic CMP gather after NMO. Note two dead and five unrecorded near-offset traces. (b) After NMO for first-order seabed peglegs and (normalized) Snell resampling.

Second, Lu et al. (1999) define offset-dependent geometric spreading corrections for a primary (g_{prim}) and its pegleg multiples (g_{mult}):

$$g_{prim} = v^* t_{prim}(\mathbf{x}) = \sqrt{(\tau v^*)^2 + \|\mathbf{x}\|^2 \left(\frac{v^*}{V_{\text{rms}}}\right)^2}, \tag{12}$$

$$g_{mult} = v^* t_{mult}(\mathbf{x}) = \sqrt{[(\tau + n\tau^*)v^*]^2 + \|\mathbf{x}\|^2 \left(\frac{v^*}{V_{eff}}\right)^2}, \tag{13}$$

where v^* is the surface velocity. We correct a pegleg for geometric spreading by applying g_{mult}/g_{prim}.

Finally, for simplicity we assume that a multiple generator's reflectivity varies in space but not in reflection angle. If $\mathbf{y}$ is the midpoint vector, let us denote $\mathbf{p}(t, \mathbf{x}, \mathbf{y})$ and $\mathbf{q}(t, \mathbf{x}, \mathbf{y})$ as small windows in time, offset, and midpoint around, respectively, a primary and its first pure multiple after normalized Snell resampling and differential geometric spreading correction. We optimize the reflection coefficient $\mathbf{r}(\mathbf{y})$ to minimize the following quadratic functional:

$$\|\text{diag}(\mathbf{p})\mathbf{r} - \mathbf{q}\|^2 + \epsilon^2 \left\|\nabla_{\mathbf{y}}^2 \mathbf{r}\right\|^2. \tag{14}$$

Operator $\nabla_{\mathbf{y}}^2$ is a 2D Laplacian, operating across the midpoint; it imposes a degree of smoothness on $\mathbf{r}(\mathbf{y})$, governed by the trade-off parameter ϵ. Using $\mathbf{x}_p$, we can compute the multiple bounce points in a 1D earth for any type of pegleg. A first-order pegleg is scaled by a single reflection coefficient, a second-order pegleg by reflection coefficients from two locations, and so on.

Pegleg imaging in a moderately heterogeneous earth

An ith-order pegleg actually consists of $i+1$ unique events. Dipping reflectors cause the events to split into individual legs (Figure 9a) on field data. Legs with a high apparent velocity hamper Radon demultiple and velocity analysis. Even if not visible, splitting can cause far-offset tuning effects between the legs, introducing a false multiple AVO signature. Therefore, to model peglegs accurately, we must extend the previous 1D theory to handle splitting.

Levin and Shah (1977) deduce moveout equations for split 2D peglegs, and Ross et al. (1999) extend the work to three dimensions. While the equations are exact in a constant-velocity earth, an extension even to $v(z)$ could prove difficult. We present a related earth-model-based imaging method called heterogeneous earth multiple NMO operator (HEMNO), which can handle variable velocity. In the small dip and constant-velocity limit, Brown (2004) shows that HEMNO reduces to Levin and Shah's result.

Figure 10 illustrates HEMNO. When reflectors dip, reflection points move both laterally and vertically. For small dips, the lateral component of reflection-point movement is negligible. We can analytically compute the location of a multiple's reflection points in a 1D earth. The basic idea of HEMNO is to measure the zero-offset traveltimes at the assumed 1D reflection points and then input those measured traveltimes to the 1D NMO for peglegs (equation 8). HEMNO requires that the earth not deviate too far from one dimensional (small dip magnitude, small lateral dip changes, small lateral velocity variation).

If τ_m is the total zero-offset traveltime of the multiple bounces along a pegleg's raypath, and τ_p is the zero-offset traveltime of the primary bounce, then we can easily extend equation 8 to HEMNO:

$$t^2 = (\tau_m + \tau_p)^2 + \frac{\|\mathbf{x}\|^2}{V_{eff}^2}. \tag{15}$$

For the particular case of the S102G pegleg, illustrated in Figure 6,

$$\tau_m = \tau^*\left(y_0 - \frac{\mathbf{x}_p}{2}\right) \quad \text{and} \quad \tau_p = \tau\left(y_0 + \frac{(\mathbf{x} - \mathbf{x}_p)}{2}\right). \tag{16}$$

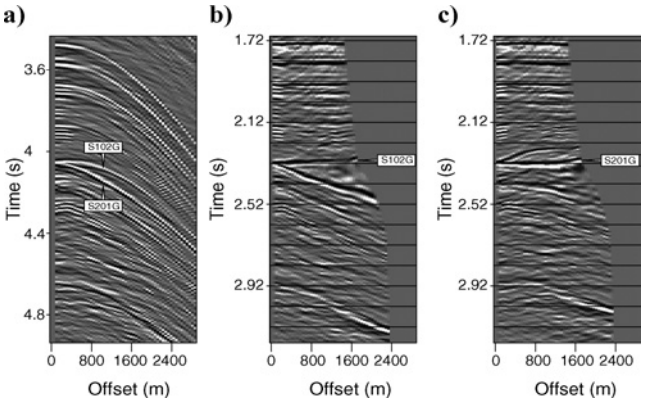

Figure 9. (a) Real CMP gather with split first-order top-of-salt pegleg (labels indicate the two legs). Pegleg apexes shift away from zero offset. (b) and (c) HEMNO (plus previous amplitude corrections) applied to the two legs.

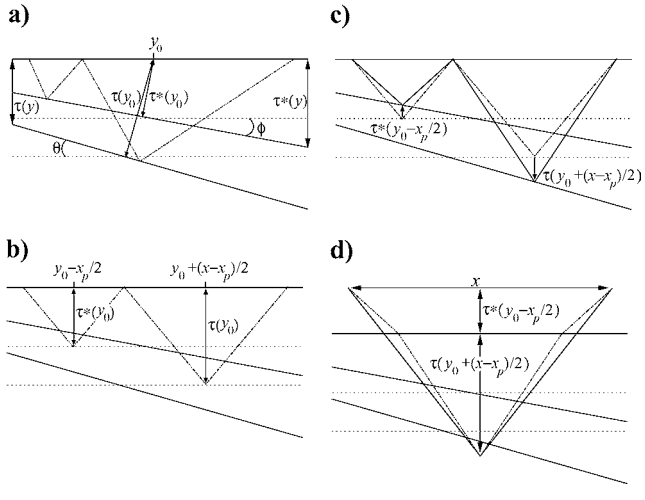

Figure 10. HEMNO schematic. (a) True S102G pegleg raypath. (b) Assumed 1D earth reflection points. (c) Raypath stretched vertically to match measured $\tau^*[y_0 - (x_p/2)]$ and $\tau(y_0 + [(\mathbf{x} - \mathbf{x}_p)/2])$. (d) Legs of composite raypath connected; solid line is final result.

Relations for other pegleg types are readily derived. Figure 9b and c show that HEMNO can independently flatten each leg of a first-order split salt-related pegleg when the salt geometry obeys HEMNO's dip assumptions.

Implementation of equation 15 requires two quantities: τ_m, obtained by hand or autopicking, and, more challengingly, τ_p, an arbitrary reflector's zero-offset traveltime. We obtain τ_p automatically by event tracking, using measured zero-offset reflector dip, which can be estimated automatically (Fomel, 2002) or manually with picked reflectors and spline interpolation (Brown, 2004).

Combined imaging/modeling operator

Now that we have defined a kinematic multiple imaging operator and a suite of amplitude-correction operators, we can define $\mathbf{L}_{i,k,m}$. We map the primary image $\mathbf{m}_0$ into data space $\mathbf{d}_0$ by applying the adjoint of normal moveout $\mathbf{N}_0$. We map the pegleg image $\mathbf{m}_{i,k,m}$ into data space $\mathbf{d}_{i,k,m}$ by applying the differential-geometric-spreading correction $\mathbf{G}_{i,m}$, Snell resampling $\mathbf{S}_{i,m}$, HEMNO $\mathbf{N}_{i,k,m}$, and reflection coefficient $\mathbf{R}_{i,k,m}$:

$$\mathbf{d}_0 = \mathbf{N}_0\mathbf{m}_0 = \mathbf{L}_0\mathbf{m}_0, \tag{17}$$

$$\mathbf{d}_{i,k,m} = \mathbf{R}_{i,k,m}\mathbf{N}_{i,k,m}\mathbf{S}_{i,m}\mathbf{G}_{i,m}\mathbf{m}_{i,k,m} = \mathbf{L}_{i,k,m}\mathbf{m}_{i,k,m}. \tag{18}$$

Equation 18 retains distinct computational advantages. Since the operator images peglegs with a vertical stretch, it is efficient to apply (important in iterative inversion), is robust to poor crossline sampling (the norm with 3D data), and allows the LSJIMP model space to consist of one midpoint location only (advantageous for parallel computing), which allows the amplitude component of the operator to be intuitive and effective. However, this pegleg modeling/imaging strategy begins to break down when reflectors dip strongly (>5°), when dips change rapidly, and when large velocity contrasts are present. It cannot model diffracted multiples; it ignores the relative shift in reflection point of a primary and the primary bounce of a pegleg.

Extension to three dimensions

A common geometry for 3D marine speculative data consists of sail-line spacing chosen just small enough to ensure even crossline midpoint coverage. Ignoring cable feathering, the crossline offset axis in this geometry contains only one live bin per common-midpoint (CMP) gather, so a CMP gather is effectively two-dimensional, allowing us to reduce the size of the LSJIMP model space by the number of crossline offset bins and greatly speeding up our LSJIMP implementation's performance. We are still imaging the multiples in a 3D sense, since (1) HEMNO uses reflector geometries measured from a 3D zero-offset section, and (2) we supply the nonzero crossline offset of the assumed 2D CMP gathers.

FIELD DATA RESULTS

WesternGeco released 2D data from Mississippi Canyon, Gulf of Mexico, for multiple-suppression benchmarking. Figure 11 shows that the data contain a variety of strong surface-related multiples that hamper interpretation.

Multiple-prediction benchmark

We can use our multiple-imaging/modeling operator to predict multiples, given a prior estimate of the primaries, similar to the crosstalk prediction of equation 6. A simple primary estimate comes by applying NMO to the data: $\mathbf{N}_0^T\mathbf{d}$. The predicted multiples $\mathbf{d}_{mult}$ are computed by modeling each pegleg and summing:

$$\mathbf{d}_{mult} = \sum_{i=1}^{p}\sum_{k=0}^{i}\sum_{m=1}^{n_{surf}} \mathbf{R}_{i,k,m}\mathbf{N}_{i,k,m}\mathbf{S}_{i,m}\mathbf{G}_{i,m}\mathbf{N}_0^T\mathbf{d}. \tag{19}$$

To benchmark the accuracy of our multiple imaging/modeling operator against an industry standard, in Figures 12 and 13 we compare equation 19's predicted multiples with those predicted by one convolution of the surface-related multiple elimination (SRME) method (Verschuur et al., 1992) on 2D Mississippi Canyon field data.

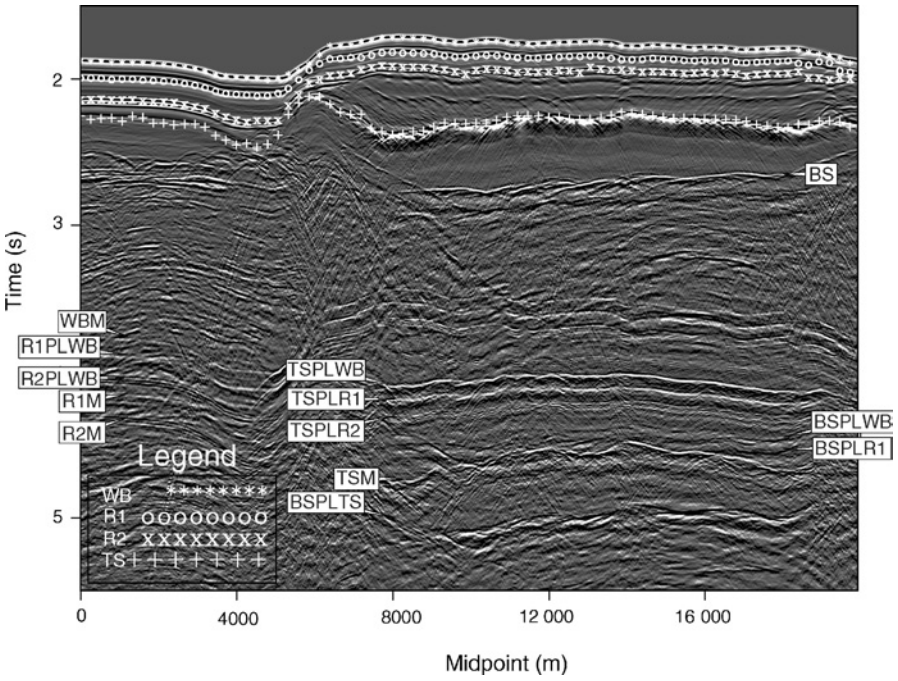

Figure 11. Stacked 2D Gulf of Mexico data, after automatic gain control. Picks denote the four multiple generators: water bottom (WB), R1, R2, and top of salt (TS). For a pure first-order water-bottom (WB) multiple, the naming convention is WBM. For a pegleg multiple with a target reflection of the top of salt (TS) and the multiple bounce on the water bottom (WB), the naming convention is TSPLWB.

Figure 12 shows a CMP gather with strong top-of-salt multiples, including the train of split peglegs between $\tau = 4.0$ and 4.3 s. Both approaches accurately model the multiple splitting. Our method's predicted multiples generally reproduce the offset-dependent amplitude and wavelet of the multiples in the data. Figure 13 shows a medium-offset slice. SRME accurately predicts the split peglegs. Our method performs well in some areas (circle) but underperforms (tall oval) where dips steepen or change rapidly. SRME predicts diffracted events (flat oval), which our method does not.

These examples show that away from complex geology, our multiple-imaging/modeling strategy can accurately transform primaries into events resembling pegleg multiples. It follows that our method can transform pegleg multiples into events comparable with primaries — a principal criterion that any LSJIMP multiple-imaging/modeling pair must satisfy.

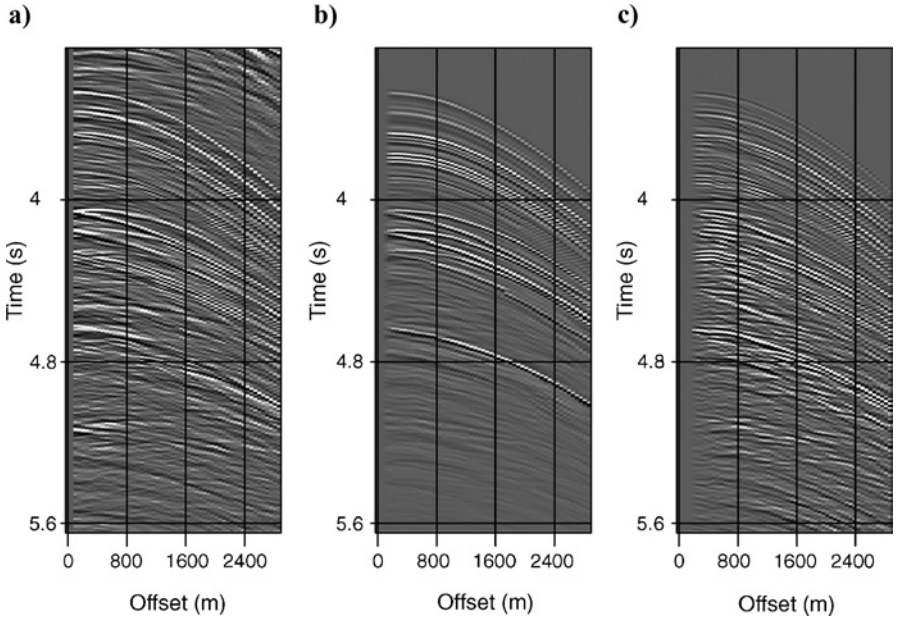

Figure 12. (a) Raw CMP gather (CMP = 9150 m). (b) Our predicted multiples. (c) SRME predicted multiples.

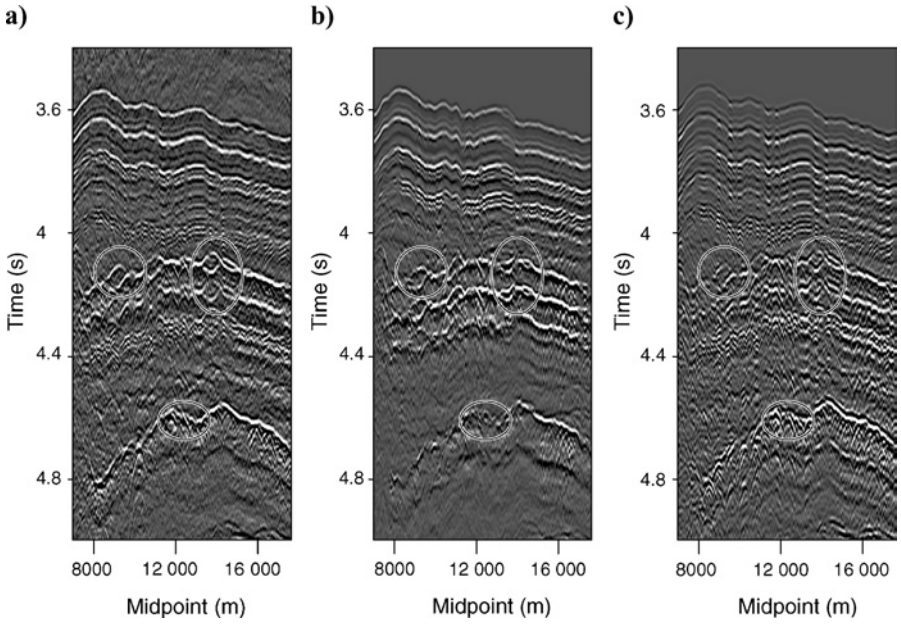

Figure 13. (a) Raw medium-offset section. (b) Our predicted multiples. (c) SRME predicted multiples.

2D LSJIMP field data results

We tested our particular LSJIMP implementation on 750 CMPs of the 2D data, modeling only first-order multiples from the four labeled multiple generators in Figure 11 ($p = 1$, $n_{surf} = 4$ in equation 1). We ran 20 conjugate gradient iterations.

Figure 14 shows stacks of the raw data after NMO, the LSJIMP estimated primary image ($\mathbf{m}_0$), and the difference between the two. LSJIMP cleanly separates primaries from a variety of surface-related multiples. However, much subsalt (midpoints >6000 m) multiple energy remains for a variety of reasons, especially salt rugosity, which causes diffracted multiples and complex focusing — neither of which HEMNO can handle. Still, our LSJIMP implementation effectively removes the specular components of most strong, salt-related multiples without harming primaries. In general, increasing the trade-off parameters ϵ_1, ϵ_2, and ϵ_3 in equation 7 removes more multiple energy from $\mathbf{m}_0$ at the cost of harming primary signal.

Figure 15 shows prestack LSJIMP results at a single CMP location over the salt (midpoint = 9150 m). Figure 15c, d, g, and h show the estimated total first-order pegleg from the seabed, $R1$, $R2$, and top-of-salt reflectors, respectively. For example, to compute the estimated seabed pegleg (Figure 15c), we construct a vector:

$$\mathbf{m}_{wb} = [\mathbf{0}\ \ \mathbf{m}_{1,0,1}\ \ \mathbf{m}_{1,1,1}\ \ \mathbf{0}\ \ \mathbf{0}\ \ \mathbf{0}\ \ \mathbf{0}\ \ \mathbf{0}\ \ \mathbf{0}]^T, \tag{20}$$

where vector $\mathbf{0}$ has the same dimension as a CMP gather and $\mathbf{m}_{1,0,1}$ and $\mathbf{m}_{1,1,1}$ are the seabed source and receiver pegleg images. We apply the LSJIMP forward model to compute the total first-order seabed pegleg:

$$\mathbf{d}_{wb} = \mathbf{L}\mathbf{m}_{wb}. \tag{21}$$

The modeled data (Figure 15e) are the sum of the estimated primaries (Figure 15b) and Figure 15c, d, g, and h. The residual error (Figure 15f) is the difference between the input data and the modeled data.

Since there are no flat events on the residual (Figure 15f) we conclude that LSJIMP preserves obscured primaries such as those seen between 3.5 and 4.0 s in (Figure 15b). Comparing Figure 15a and e, note that even the complex, visibly split salt-related multiples are modeled and separated fairly well. However, the multiples remaining in the residual Figure 15f imply that the forward model has not perfectly modeled the physics of the multiples. The LSJIMP model-regularization operators have interpolated the missing near-offset information.

Figure 16 compares the results of LSJIMP and a least-squares, high-resolution Radon demultiple [see Trad et al. (2003) for a review] on the CMP gather at the same location as in Figure 15. The high apparent velocity of one leg of the split top-of-salt pegleg (circled in Figure 16b) significantly degrades a Radon demultiple's ability to attenuate it. LSJIMP directly models splitting behavior of the event and can thus better separate it from the estimated primaries.

3D LSJIMP field data results

Compagnie Générale de Géophysique (CGG) acquired a 3D speculative survey in the Gulf of Mexico's Green Canyon. We processed a small subset (192 by 14 CMP locations) with nontrivial crossline dip (>3°) extracted from a sedimentary minibasin. As noted earlier, we ignored the crossline offset axis of the data, leaving a 4D prestack data cube and thereby strongly accelerating LSJIMP's performance.

Figure 17 zooms into the multiple-infested zone before and after LSJIMP. Stacking mostly suppresses multiples; but from the difference panel (Figure 17c), note that LSJIMP nonetheless subtracts much remaining multiple energy without seriously harming primaries. The time slice on the 3D cube transects a strong seabed pegleg; it shows up prominently on the raw data stack and the difference panel but is largely absent from the LSJIMP estimated primaries stack.

Figure 18 shows LSJIMP's performance on a CMP gather (for a single nonzero

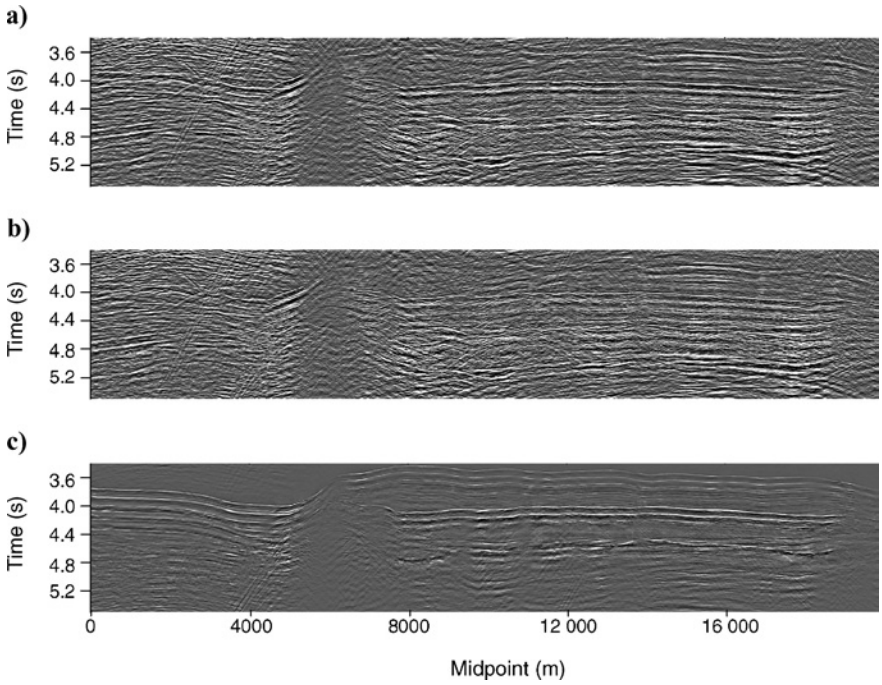

Figure 14. Stacked images before and after LSJIMP. All panels gained with t^2 and clipped to same level. (a) Raw data. (b) LSJIMP estimated primaries $\mathbf{m}_0$. (c) Difference.

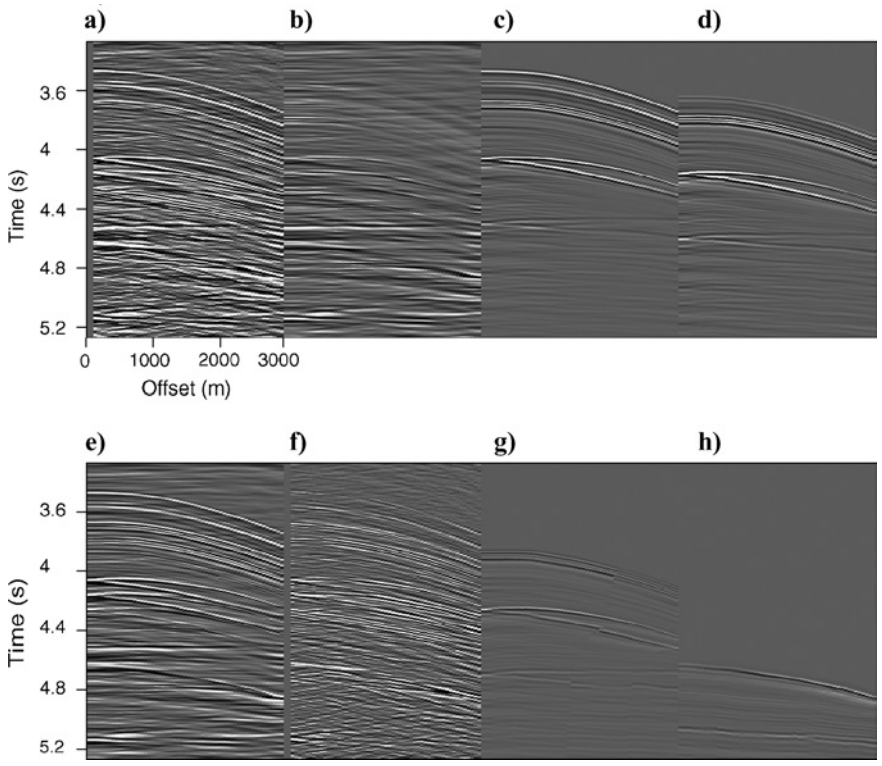

Figure 15. Two-dimensional Gulf of Mexico CMP 344 (9150 m) before and after LSJIMP. Panels are defined in text. All panels are NMO'ed, windowed from 3.5 to 5.5 s, and gained with t^2 for ease of viewing.

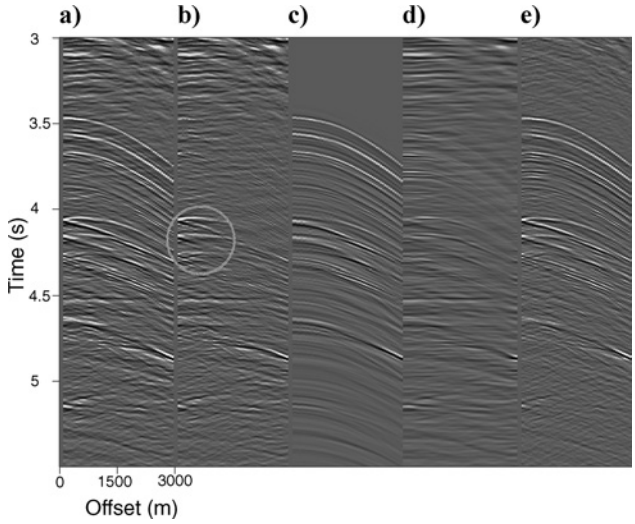

Figure 16. LSJIMP versus least-squares, high-resolution hyperbolic Radon demultiple on CMP 344 (9150 m) of the Mississippi Canyon 2D data set. (a) Raw data. (b) Radon estimated primaries. (c) Radon estimated multiples. (d) LSJIMP estimated primaries. (e) LSJIMP estimated multiples.

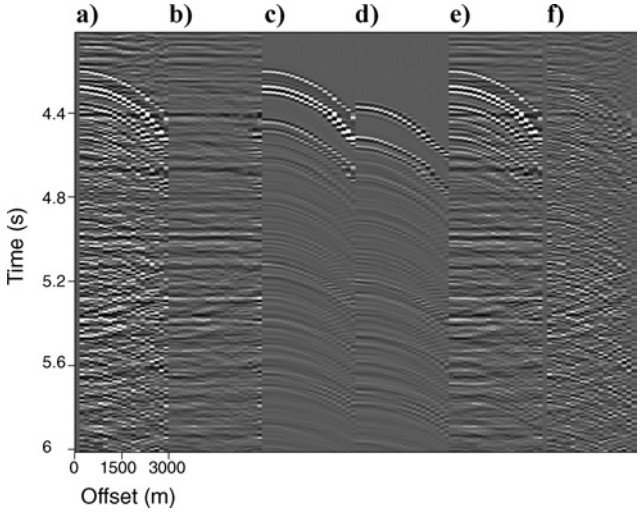

Figure 18. LSJIMP results on individual midpoint location (CMP $x = 100$; CMP $y = 4$). Panels are defined in text. All panels are NMO'ed, windowed in time from 4.0 to 6.0 s, and gained with t^2 for ease of viewing.

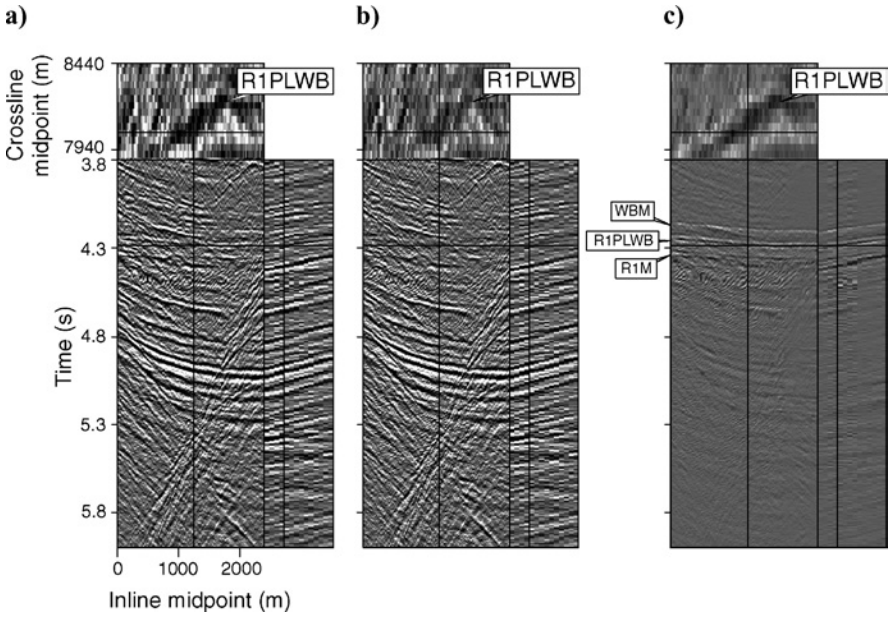

Figure 17. Zoom of stacked subset of CGG 3D data before and after LSJIMP. All panels are windowed in time from 4.0 to 5.0 s. (a) Raw data stack. (b) Stack of estimated primary image $\mathbf{m}_0$. (c) Stack of the subtracted multiples.

crossline offset). Note strong multiples at $\tau = 4.3$ s in the raw data (Figure 18a) and primaries under the multiple curtain. The LSJIMP-estimated primaries (Figure 18b) are effectively free of multiples; moreover, since the data residual (Figure 18f) contains little correlated energy, we have preserved the primaries and effectively modeled the important multiples (Figure 18c and d).

CONCLUSIONS

The LSJIMP method, a general least-squares inversion algorithm, simultaneously combines images of multiples and primaries and suppresses the crosstalk noise that inhibits simple image averaging. LSJIMP's novelty lies in the three model-regularization operators that suppress crosstalk and exploit the redundancy within and between images to increase signal fidelity.

We presented a particular LSJIMP implementation that uses a relatively simple time-domain, true-relative-amplitude imaging operator for pegleg multiples. While our pegleg-imaging/modeling scheme is limited to specularly reflected multiples from mildly dipping reflectors, we demonstrate on a 2D field data example that our method can accurately model salt-related split peglegs. Moreover, the method is robust to sparse 3D marine geometries and computationally efficient, which is crucial for iterative inversion.

Tests on real 2D and 3D marine field data examples confirm that LSJIMP holds promise as a novel and useful tool in the quest to fully exploit more of the unused information in the seismic wavefield. In both cases, LSJIMP separates primaries from a variety of surface-related pegleg multiples. While the separation is not perfect, the amplitude of primaries is nonetheless preserved. Information from the multiples helps to constrain missing near-offset primary information. On the 2D example, we compared LSJIMP to a high-resolution

hyperbolic Radon demultiple and found that LSJIMP separated a split salt-related pegleg from the data better than the Radon demultiple.

Looking ahead, we note that the continued trend toward inexpensive parallel computing may soon allow LSJIMP implementations with more accurate (and expensive) prestack imaging operators for multiples. LSJIMP shows great promise to jointly image other important wave modes often seen in data. Local shear-wave conversions and internal multiples may offer valuable information in the subsalt imaging problem; these modes fit the one data record, many data sets model of LSJIMP. Extensions to LSJIMP for multicomponent data are possible.

ACKNOWLEDGMENTS

Thanks go to WesternGeco and Compagnie Générale de Géophysique (CGG) for acquiring and releasing the field data shown in this paper, as well as the sponsors of the Stanford Exploration Project for financial and technical support. This work benefited from useful discussions and support from Robert Clapp, Biondo Biondi, and Clement Kostov as well as from thoughtful and patient reviews by the associate editor and two anonymous reviewers.

REFERENCES

Berkhout, A. J., and D. J. Verschuur, 1994, Multiple technology, part 2: Migration of multiple reflections: 64th Annual International Meeting, SEG, Expanded Abstracts, 1497–1500.

———, 2003, Transformation of multiples into primary reflections: 73rd Annual International Meeting, SEG, Expanded Abstracts, 1925–1928.

Berryhill, J. R., and Y. C. Kim, 1986, Deep-water peglegs and multiples — Emulation and suppression: Geophysics, **51**, 2177–2184.

Brown, M. P., 2004, Least-squares joint imaging of multiples and primaries: Ph.D. dissertation, Stanford University.

Claerbout, J. F., 1992, Earth soundings analysis: Processing versus inversion: Blackwell Scientific Publications, Inc.

Fomel, S., 2002, Applications of plane-wave destruction filters: Geophysics, **67**, 1946–1960.

Guitton, A., 2002, Shot-profile migration of multiple reflections: 72nd Annual International Meeting, SEG, Expanded Abstracts, 1296–1299.

Guitton, A., M. Brown, J. Rickett, and R. Clapp, 2001, Multiple attenuation using a *t-x* pattern-based subtraction method: 71st Annual International Meeting, SEG, Expanded Abstracts, 1305–1308.

He, R., and G. Schuster, 2003, Least-squares migration of both primaries and multiples: 73rd Annual International Meeting, SEG, Expanded Abstracts, 1035–1038.

Kuehl, H., and M. Sacchi, 2001, Generalized least-squares DSR migration using a common angle imaging condition: 71st Annual International Meeting, SEG, Expanded Abstracts, 1025–1028.

Levin, F. K., and P. M. Shah, 1977, Peg-leg multiples and dipping reflectors: Geophysics, **42**, 957–981.

Lu, G., B. Ursin, and J. Lutro, 1999, Model-based removal of water-layer multiple reflections: Geophysics, **64**, 1816–1827.

Morley, L., 1982, Predictive multiple suppression: Ph.D. dissertation, Stanford University.

Nemeth, T., C. Wu, and G. T. Schuster, 1999, Least-squares migration of incomplete reflection data: Geophysics, **64**, 208–221.

Prucha-Clapp, M., and B. Biondi, 2002, Subsalt event regularization with steering filters: 72nd Annual International Meeting, SEG, Expanded Abstracts, 1176–1179.

Reiter, E. C., M. N. Toksöz, T. H. Keho, and G. M. Purdy, 1991, Imaging with deep-water multiples: Geophysics, **56**, 1081–1086.

Riley, D. C., and J. F. Claerbout, 1976, 2-D multiple reflections: Geophysics, **41**, 592–620.

Ross, W. S., Y. Yu, and F. A. Gasparotto, 1999, Traveltime prediction and suppression of 3-D multiples: Geophysics, **64**, 261–277.

Sava, P., and S. Fomel, 2003, Angle-domain common-image gathers by wavefield continuation methods: Geophysics, **68**, 1065–1074.

Shan, G., 2003, Source-receiver migration of multiple reflections: 73rd Annual International Meeting, SEG, Expanded Abstracts, 1008–1011.

Tarantola, A., 1987, Inverse problem theory: Methods for data fitting and model parameter estimation: Elsevier Science Publ. Co., Inc.

Trad, D., T. Ulrych, and M. Sacchi, 2003, Latest views of the sparse Radon transform: Geophysics, **68**, 386–399.

Tsai, C. J., 1985, Use of autoconvolution to suppress first-order long-period multiples: Geophysics, **50**, 1410–1425.

Verschuur, D. J., A. J. Berkhout, and C. P. A. Wapenaar, 1992, Adaptive surface-related multiple elimination: Geophysics, **57**, 1166–1177.

Wang, J., H. Kuehl, and M. Sacchi, 2003, Least-squares wave-equation AVP imaging of 3D common azimuth data: 73rd Annual International Meeting, SEG, Expanded Abstracts, 1039–1042.

Wang, Y., 2003, Multiple subtraction using an expanded multichannel matching filter: Geophysics, **68**, 346–354.

Wiggins, J. W., 1988, Attenuation of complex water-bottom multiples by wave equation-based prediction and subtraction: Geophysics, **53**, 1527–1539.

Yu, J., and G. Schuster, 2001, Crosscorrelogram migration of IVSPWD data: 71st Annual International Meeting, SEG, Expanded Abstracts, 456–459.